Progress in Superconductivity Vol.14 No.2 pp.87-91 31 December 2012

Thermal and Non-thermal Heat Flow in a Large Crystal Detector for Neutrinoless Double Beta Decay Search

G. B. Kim[a,b], S. J. Lee[+,a], Y. S. Jang[a], H. J. Lee[a], J. H. Lee[a,b], J. Y. Lee[a], M. K. Lee[a], W. S. Yoon[a] and Y. H. Kim[*,a]

[a] *Korea Research Institute of Standard Science, Daejeon, Korea*

[b] *Seoul National University, Seoul, Korea*

(Received 17 December 2012; revised 20 December 2012; accepted 24 December 2012)

Abstract

Metallic magnetic calorimeters (MMCs) are one of the most competitive low temperature detector (LTD) readout sensors. They have the advantages of high time resolution, no heat dissipation, and a wide range of operating temperature. We apply MMCs to our neutrinoless double beta decay (0νββ) search experiment. A $CaMoO_4$ crystal was employed as both a source of 0νββ and an energy absorber. The crystal was thermally connected to a MMC sensor. We set a simple thermal model for this detector and measured pulse shapes are compared with a numerical solution of the thermal model.

Keywords : Magnetic Calorimeter, Low Temperature Detector, Thermal model.

I. Introduction

The mass and the basic property of neutrinos have been major problems of fundamental particle physics during the past two decades. Currently, searching for neutrinoless double beta decay (0νββ) [1, 2] is a key experiment in determining the effective mass of electron neutrinos, if they have finite mass and are self-antiparticles - the so called Majorana particles [3]. Because the half-life of the decay is proportional to inverse-square of the effective mass, the 0νββ process is extremely rare. Several experimental techniques are considered to increase the sensitivity of probing this rare process. Increasing the detector mass for a large number of 0νββ candidates is one of these efforts. Reducing internal and external background signals is an essential effort for the experiment. Increasing the energy resolution of the detector is another strategy to increase the sensitivity in this kind of rare event search. Here, our experimental work is to develop high resolution detectors using a low temperature detector (LTD) for 0νββ search.

The AMoRE (Advanced Mo based Rare process Experiment) project [4], an international collaboration on 0νββ experiment, uses $CaMoO_4$ scintillating crystals [5] as a source of ^{100}Mo decays and an absorber for the two electrons from the decay. The project plans a cryogenic experiment for strong advantages of LTDs for the rare event search. Thanks to their high energy resolution, efficient signal selections from background noise can be achieved to obtain high experimental sensitivity in the energy region of interest. We employ MMCs, which show high time resolution, no heat dissipation, and a wide range of operating temperature [6].

*Corresponding author. Tel : +82 42 868 5975

e-mail : yhkim@kriss.re.kr

+ Now belong to NASA/Goddard Space Flight Center.

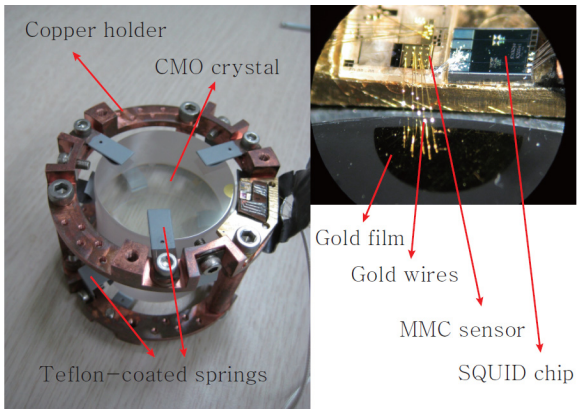

Fig. 1. Our detector is shown in the left picture. In the upper–right, an enclosed view of the MMC sensor is also shown.

To make a detector with the best condition for 0νββ search, one of the most important experimental procedures is the design of the detector for optimal sensitivity. It is essential to understand thermal physics of the detector for optimization. After particle absorption, thermalization processes and heat flow mechanisms in the detector components have to be clarified. In this study, we set a simple thermal model. The measured temperature signals are compared with the analytical solutions of the model to understand heat flow in the detector.

II. Detector set-up

A cylindrical $CaMoO_4$ crystal with a diameter of 4 cm and a height of 4 cm was used as the main detector as shown in Fig. 1. The crystal was held by phosphor-bronze springs attached to a ring type copper holder. To make a thermal connection between the sensor and the absorber, a thin gold film was evaporated on the crystal surface. Gold bonding wires were attached to the gold film and the MMC sensor. A meander type superconducting pickup loop for the MMC sensor was connected to input pads of a current-sensing dc-SQUID. A magnetization change of the MMC induces current change in the superconducting loop. Details of the MMC sensor wiring and the measurement principle are described in our earlier work [7].

An external ^{210}Po source was attached to the copper holder in this run, and a detector assembly was attached to the mixing chamber of a dilution refrigerator.

III. Thermal model

We established a simple thermal model to understand heat flow in the detector as illustrated in Fig. 2. The model is described with two major thermal components, the $CaMoO_4$ crystal and the MMC sensor. The gold film is considered as an intermediate thermal stage. The phonons in the gold film are connected with the phonon system in the crystal. On the other hand, the electrons in the film are thermally attached to the MMC sensor via gold bonding wires. C_c and C_M stand for the heat capacities of the crystal and the MMC, respectively, while G_K, G_{ep}, G_{cg}, G_{gm}, G_{cb}, and G_{mb} describe thermal conductance between the parts in the diagram.

Practically, we measure the temperature of the MMC sensor, and compare it with the numerical solution of combined differential equations associated with the thermal model in order to clarify the heat flow mechanism.

After particle absorption in the crystal, phonons with an energy level close to Debye energy are initially created and are down-converted to lower energy phonons via anharmonic processes. When their energy reaches 20~50 K, these phonons can have a significantly long life time to travel ballistically around the crystal without decaying. They do not follow the thermal phonon distribution for a given temperature. The life time of the non-thermal phonons depends upon surface conditions, impurities, crystality, and geometry of the crystal.

In the present experiment, a significant portion of the non-thermal phonons hitting the gold film can interact with electrons in the thin gold film. In this case, the energy of a non-thermal phonon is

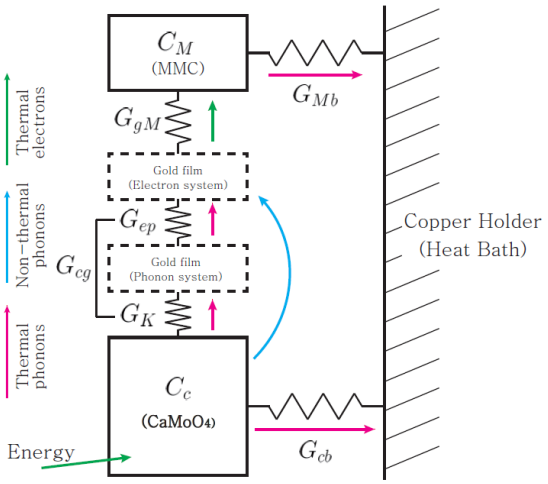

Fig. 2. Our thermal model for the detector. The red, blue, and green lines indicate heat transfer by non-thermal phonons, thermal phonons, and thermal electrons, respectively. *C*'s and *G*'s correspond to heat capacity and thermal conductance values. The physical meaning and the calculated and measured values of the parameters are listed in the table 1.

transferred into the electron system in the gold film. Remaining non-thermal phonons are down-converted further over time by inelastic scattering processes. Normally, this thermalizing time takes a few milliseconds. After thermalization, the crystal is filled with thermal phonons. These processes lead to the crystal and the gold film settling at different temperatures higher than the bath temperature. Then, the heat flows through each of the thermal components following the second law of thermodynamics toward the heat bath.

The flow between the lattice of the crystal and that of the gold film can be understood by an acoustic mismatch model (i.e. Kapitza conductance) [8]. Thermal phonons, then, interact with thermal electrons in the gold film by electron-phonon coupling [9]. At low temperatures, the electron-phonon interaction becomes weak and results in inefficient heat flow. It can be a major thermal impedance of the thermal process below 50 mK. The gold bonding wires are responsible for the heat flow between thermal electrons in the gold film and the MMC sensor. The electronic thermal conductance of gold wires can be described by the Wiedemann-Franz law [10].

Based on this thermal model, heat equations for the detector are written as

$$C_c\, dT_c(t) = P_c(t)\, dt - (T_c(t) - T_g(t))\, G_{cg} - (T_c(t) - T_b)\, G_{cb}, \quad (1)$$

$$0 = P_g(t)\, dt - (T_g(t) - T_c(t))\, G_{cg} - (T_g(t) - T_M(t))\, G_{gm}, \quad (2)$$

$$C_m\, dT_M(t) = - (T_m(t) - T_g(t))\, G_{cg} - (T_m(t) - T_b)\, G_{cb}, \quad (3)$$

where T_c, T_g, and T_M are the temperature of the crystal, the gold film, and the MMC, respectively. Also P_c and P_g are thermal energy input to the crystal and the gold film, respectively. Heat capacity of the gold film is ignored for simplicity. Analytical solutions for Eq. (1-3) can be found in the form of

$$T_m(t) = A\,(e^{-a\,t} - e^{-c\,t}) + B\,(e^{-c\,t} - e^{-b\,t}) + T_b, \quad (4)$$

where T_b is the base temperature of the system and the coefficients of A, B, a, b, and c are composited by thermal model parameters, C, G, E, ε, and τ, respectively. E is the total energy of phonons. ε is the fraction of the energy absorbed into the gold film via non-thermal process, and τ is the thermalizing time.

IV. Experimental result

Pulses of 5.3 MeV alpha signals from an external ^{210}Po source were averaged to make a comparison with the analytic solution of the model. A few tens of pulses without any pileup signal were averaged for measurement at each temperature, and they are converted to temperature scale of MMC to compare with the thermal model solution.

A least-squares method was performed to fit the measured pulse with the function of Eq. (4). A few parameters in the thermal model can be calculated. However, all parameters were set as free fitting

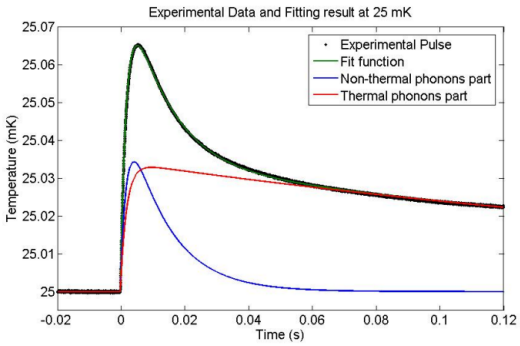

Fig. 3. The measured pulse shape at 25 mK (dot-marker) and fitting result (green). The faster (blue) and slower (red) parts of the fit function correspond to non-thermal and thermal processes of the initial heat flow.

parameters because of possible uncertainties from some material dependencies. The resulting fit shows a good agreement with the rise and decay component of the measured signal as shown in Fig. 3. The black line is an averaged pulse measured at 25 mK. The green line is the result of the fitting procedure. The parameters found by fitting with the thermal model and the expected values are listed in Table 1. It is noticeable that those values are in reasonable agreement.

Our model indicates that the initial heat flow is categorized by thermal and non-thermal processes. The fit function can also be separated into two parts. The first term on the right side of Eq. (4) is related to non-thermal phonon contribution while the second term stands for the thermal process. The non-thermal process carries a more efficient and faster heat flow than the thermal process because it is a direct energy transfer to conduction electrons in the gold film from non-thermal phonons. This process happens before the phonons are thermalized.

Fig. 3 shows the contribution of the two non-thermal and thermal processes to the measured signal. According to the fitting result in Table 1, only 7.7 % of the total deposited energy was absorbed directly into the gold film from the non-thermal process. However, the signal height resulted almost equally from the two processes.

The detector can be further optimized taking into account the efficient non-thermal process. For example, the size and thickness of the gold film can change the collection and absorption efficiency of the non-thermal phonons.

Table 1. Parameters expected and found with the model. τ is the thermalizing time of phonons in the crystal, and ε is the fraction of the energy absorbed into the gold film via the non-thermal process. E is the total energy deposited in form of phonons. A 5% light yield is assumed in the E calculation.

Parameters	Calculated value	Fit value
C_c (J/K)	2.37×10^{-9}	2.33×10^{-9}
C_M (J/K)	7.58×10^{-10}	7.36×10^{-10}
G_{cg} (W/K)	4.85×10^{-9}	5.99×10^{-9}
G_{gm} (W/K)	2.10×10^{-7}	2.87×10^{-7}
G_{cb} (W/K)	None	3.08×10^{-9}
G_{mb} (W/K)	None	5.23×10^{-8}
E (J)	8.06×10^{-13}	8.08×10^{-13}
ε (unitless)	None	7.66×10^{-2}
τ (s)	None	1.94×10^{-3}

V. Conclusion

We examined thermal and non-thermal processes of heat flow in a detector composed of a $CaMoO_4$ crystal and a MMC sensor. A simple thermal model is established to describe the measured temperature signals. Based on the physical properties of parameters, such as the size and thickness of the gold film, the size of the MMC sensor, and the method of thermal connection to the bath, detector performance can be further improved.

Since $CaMoO_4$ scintillates, additional detectors to measure the light originating from particle absorption can be introduced together with a phonon sensor developed in the current research. In future research, the possibility of different light yields for alpha and electron events will be investigated to distinguish $0\nu\beta\beta$ signals from background alpha events.

References

[1] Bilenky, S. M. Physics of Particles and Nuclei 41, 5,

690-715 (2010).
[2] Zuber, K., arXiv preprint nucl-ex/0610007 (2006).
[3] Majorana, E., Nuovo Cim. 14, 171 (1937).
[4] Bhang, H., et al. J. Phys.: Conf. Ser. 375 042023 (2012).
[5] Annenkov, A. N., et al. Nucl. Istr. Meth. A, 584, 2, 334-345 (2008).
[6] Burck, A., et al. J. Low Temp. Phys., 151, 1, 337-344 (2008).
[7] Yoon, W. S., et al. J. Low Temp. Phys., 167, 2, 280-285 (2012).
[8] Kapitza, P. L., Phys. Rev. 60, 354 (1941).
[9] Hopkins, P. E., et al. J. Appl. Phys. 105, 023710 (2009).
[10] Franz, R. and Wiedemann, G., Ann. Phys., 165, 497-531 (1853).